Viscous damping and spring force in periodic perforated planar microstructures when the Reynolds' equation cannot be applied

Dorel Homentcovschi[a] and Ronald N. Miles
Department of Mechanical Engineering, State University of New York, Binghamton, New York 13902-6000

(Received 15 July 2009; revised 13 October 2009; accepted 14 December 2009)

A model of squeeze-film behavior is developed based on Stokes' equations for viscous, compressible isothermal flows. The flow domain is an axisymmetrical, unit cell approximation of a planar, periodic, perforated microstructure. The model is developed for cases when the lubrication approximation cannot be applied. The complex force generated by vibrations of the diaphragm driving the flow has two components: the damping force and the spring force. While for large frequencies the spring force dominates, at low (acoustical) frequencies the damping force is the most important part. The analytical approach developed here yields an explicit formula for both forces. In addition, using a finite element software package, the damping force is also obtained numerically. A comparison is made between the analytic result, numerical solution, and some experimental data found in the literature, which validates the analytic formula and provides compelling arguments about its value in designing microelectomechanical devices.
 [DOI: 10.1121/1.3290990]

PACS number(s): 43.38.Bs, 43.38.Kb [AJZ] Pages: 1288–1299

I. INTRODUCTION

Recent progress in micromachining technology has enabled the fabrication of microelectromechanical systems (MEMS), such as microphones, microaccelerometers, pressure sensors, switches, mirrors, tunable interferometers, ultrasonic motors, resonators, etc. MEMS devices often use parallel plate electrodes as the capacitive sensing and electrostatic actuation mechanisms. This is why the study of a thin air layer being squeezed between a vibrating plate and a rigid plate, referred to as a planar microstructure, is important in many microelectromechanical systems. As the movable electrode displaces sinusoidally, the backforce on the plate due to the air separating it from the backplate has two components Ref. 1: the viscous damping force, which is in phase with velocity, and the spring force, which is in phase with the plate displacement. While the compressibility of the gas and inertial forces become important factors in determining the spring force at higher frequencies, the viscous forces dominate the mechanical behavior of planar microstructures at low frequencies. This paper is focused mainly on determining the viscous damping in planar, periodic perforated microstructures acting at audible frequencies.

The rigid backplate often contains numerous perforated holes which are of a few microns in diameter, uniformly distributed over the entire backplate, for reducing the time required to remove sacrificial materials between the moving structure and backplate during the wet etching process. A thicker backplate is usually preferred since it can provide much better stability and mechanical rigidity. The quasihorizontal motion of the air in the thin gap in a planar microstructure yields squeeze-film damping that can adversely affect the dynamic response of the device. Thus, in the case of microphones (and also other sensors designed for small signal applications), the mechanical-thermal noise is often one of the limiting noise components. The magnitude of thermal noise depends only on temperature and the magnitude of mechanical damping, high viscous damping being associated with large mechanical-thermal noise.[2] The perforations in one of the plates can be also used to control the viscous damping. As a result there is an extensive literature dedicated to the study of squeeze-film damping in perforated MEMS.[3–7]

While the squeeze-film damping is reduced by incorporating holes in one plate, the vertical motion of the air within the holes gives a new viscous resistance which adds to the squeeze-film damping. A rigorous solution of the total damping problem requires the solution of the Navier–Stokes' (NS) system in the three-dimensional (3D) domain comprised of the space between the plates and the volume of the holes, which is not at all a simple task. Three-dimensional flow simulations are not practical for the entire microstructure geometry[5] due to the complexity of the implementation and the computational resource requirements.

There is a large body of modeling work based on the lubrication approximation. The lubrication approximation assumes that the distance between the plane surfaces is sufficiently small, such that it is possible to integrate the NS equations over the separation distance to obtain a two-dimensional (2D) equation for pressure widely known as the Reynold's equation. In the case of perforated microstructures, the assumption that the flow domain is thin is not valid in the region of holes. As a result, the Reynold's equation

[a]Permanent address: "Politechnica" University of Bucharest and Institute of Mathematical Statistics and Applied Mathematics of Romanian Academy, Calea13 Septembrie #13, RO-76100, Bucharest, Romania. Author to whom correspondence should be addressed. Electronic mail: homentco@binghamton.edu

cannot be applied if the air gap between the planes and the pitch and radius of holes have comparable geometrical dimensions. For this case, the widely used Reynold's equation (whose solution gives Škvor's formula[8]) may not be appropriate without significant modifications.

There are two ways to overcome the difficulties associated with the application of the Reynold's equation in perforated microstructures. The first one is to add new terms and coefficients in order to account for the influence of holes, the open end of the holes, the bending of flow from horizontal to vertical. Modifications to the Reynolds' equation have been made by adding a term related to the damping effect of gas flow through holes in Refs. 9 and 10. This modified Reynold's equation was solved analytically in particular cases, but more complicated configurations require the use of numerical methods, which diminishes the utility of the lubrication approximation. In "the analytic damping model" derived in Refs. 5, 11, and 12 (see also Ref. 13), the mechanical resistance of a perforation cell consists of six lumped flow resistances. One of these resistances is derived analytically by using the Reynolds' equation. The elongations involved in the other lumped resistances contain up to 20 numerical coefficients that are determined by using some heuristic equations and fitting to finite element method (FEM) simulations. In some cases, the new models are also encumbered with a lot of experimental coefficients added to provide agreement between the numerical and experimental results as in Refs. 14 and 15. All these methods developed for determining the damping force (and at higher frequencies also the spring force) of the oscillating perforated microstructures obtained by extending the Reynolds' equation are known as "compact models." As noted in the recent paper by Veijola *et al.*,[16] "the verification of the compact models is generally questionable."

An alternative way to determine the viscous damping of perforated microstructures when the pitch of the holes, the air gap, and the radius of holes are of the same order (when the Reynold's equation cannot be applied) is to integrate the NS system and to obtain the velocity and pressure fields. In the model developed here, we take advantage of the repetitive pattern of holes which is typical in most designs. This repetitive pattern implies the existence of a basic cell associated with each hole. For example, if the holes are aligned and regularly spaced, then the lower part of the cell (inside the gap) would be a square prism while for staggered holes, the lower part of the cell will be a hexagonal prism. Due to symmetry the normal velocity and the normal pressure derivative on each side plane of these prisms vanish. For the present model, the prismatic part of the basic cell will be approximated by a circular cylinder (of the same section area and height) having zero normal velocity along the side surface. This yields a 2D (axisymmetrical) flow problem. This approach is similar to the one used in the lubrication approximation where the original problem for a square or hexagonal domain was replaced by a problem for a circular domain which led to Škvor's formula.

The analytical solution developed in Sec. III is based on using Stokes' approximation to the Navier–Stokes system describing the motion of an isothermal, compressible fluid in the approximated cell. The resultant problem for the finite circular cylinder is similar to the flow problems studied by Robey,[17] Petritskaya,[18,19] and Zukerwar[20] for determining the theoretical response of a condenser microphone. The main result of this work is an analytical formula [Eq. (67)] for the complex force whose real part gives the viscous damping and the imaginary part is the spring force. At low frequencies (i.e., in audible domain), the viscous damping is the most important part; moreover, as was shown in Refs. 8 and 20, this component is almost independent of frequency and can be determined by a steady-state approach. This opens the possibility of determining the damping force numerically by using a finite element package for steady-state flow of compressible gas in an axisymmetrical domain.

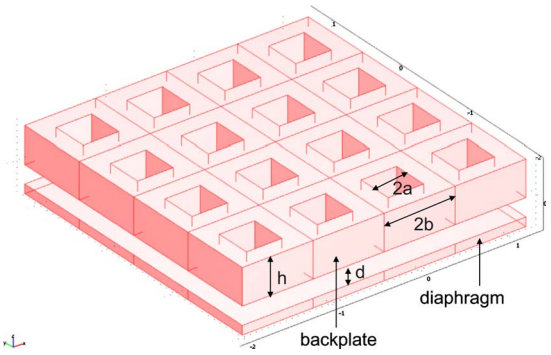

FIG. 1. (Color online) A perforated planar microstructure with aligned square holes.

The damping force given by the analytical formula is validated by results of numerical simulation and also by direct comparison with some experimental data found in the literature.

II. MODEL FORMULATION

Consider a uniform perforated (equal pitch and equal sized holes) planar microstructure having a repetitive pattern of holes. Generally, perforations are present in staggered and aligned (matrix) configurations. In the case of a staggered system of holes, a hexagonal pattern repeats while for the aligned (nonstaggered or matrix) holes, a square pattern can be noted. In Fig. 1, a regular matrix of square holes is shown. The upper plate is the perforated backplate (of thickness h) and the lower one is the diaphragm. The distance d between the average positions of the two plates is the air gap of the structure. The cylindrical holes (circular or square) lie on the vertices of a regular web of hexagons or squares of a side length denoted by $l=2b$ (the pitch of the holes) in both cases. The domain is filled by air. The geometry in the case of aligned holes (square pattern) is shown in Fig. 2. The repetitive pattern of the system of holes and the vertical motion of the diaphragm yield a similarly repetitive response in the motion of the air. The domain where a hole collects the flow will be called a cell. The basic domain for the unit cell is shown in Fig. 3. It consists of a square prism domain D_g located below the square etched cylindrical domain D_h representing the hole. All the side planes of the domain D_g are symmetry planes for the fluid motion. Consequently, on each plane surface, the normal component of velocity and the nor-

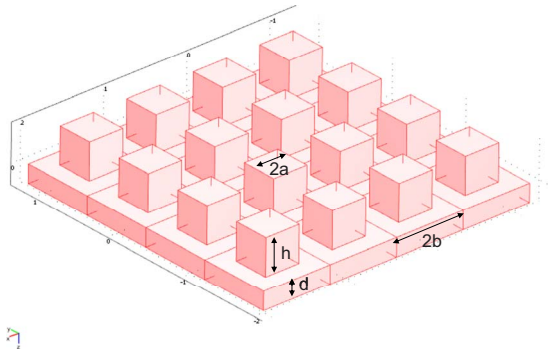

FIG. 2. (Color online) The air domain corresponding to the planar microstructure in Fig. 1.

mal pressure derivative are zero. On the other side, the velocity components vanish on the solid boundary surface of a hole (no-slip condition and no penetration conditions). Finally, the pressure on the upper base of a hole equals the external atmospheric pressure (or more generally is connected to the volume velocity by means of a known impedance Z_C of the backchamber) and the velocity on the other solid surface of the flow domain (diaphragm) equals the velocity of this surface.

In order to simplify the problem, we approximate the domain D_g by a circular cylinder C_g (see Fig. 4) of the same volume having the area of the normal section equal to the area of the hexagonal or square section of the prism D_g [the radius of the cylinder C_g is therefore $R=2b\sqrt{\sqrt{3}/(2\pi)}$ in the case of staggered holes and $R=2b/\sqrt{\pi}$ in the case of matrix holes]. The condition of vanishing of the normal velocity (and of pressure normal derivative) on all symmetry side planes will be substituted by cancellation of these quantities on the side surface of the domain C_g. The radius of the hole is denoted by r. In the case of square holes (width $2a$), as in Fig. 1, the value of r is determined by equalizing the total resistance (sum of the direct and indirect resistances from Ref. 21) for a circular hole $F^h_{\bigcirc}$ and the total resistance $F^h_{\square}$ of a square hole:

$$F^h_{\square} \equiv \frac{12}{0.4217}\mu h\left(\frac{b}{a}\right)^4 w = 8\pi\mu h\left(\frac{R}{r}\right)^4 w \equiv F^h_{\bigcirc}.$$

The resulting formula $r=1.094a$ compares well with the value $r=1.096a$ obtained in Ref. 13 by equating the acoustic

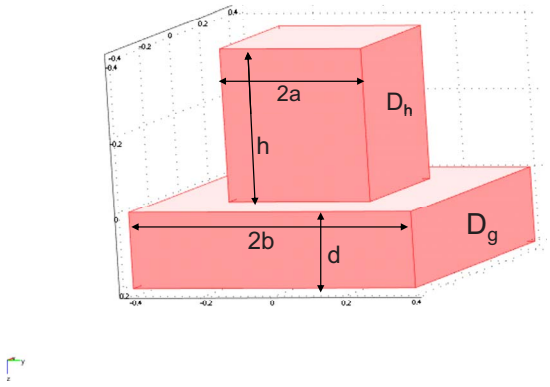

FIG. 3. (Color online) A cell of a periodic microstructure with aligned square holes.

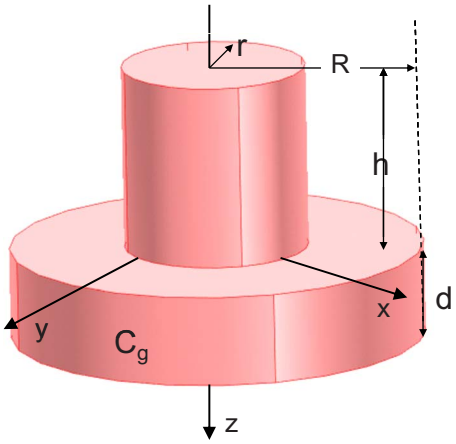

FIG. 4. (Color online) The cylindrical approximation of the basic domain (cell).

resistances (hydraulic resistances) of square and circular long channels. This approximation works in the case of small and moderate values of the area ratio A (defined as the ratio of the area of the normal section of the hole over the total area of a normal section of the domain D_g). This way we obtained an axisymmetrical problem which is easier to solve analytically and numerically.

In the case the air gap, the pitch of the holes, and the diameter of the holes are all of the same order, the lubrication approximation can no longer be used. Therefore, we no longer have a special equation for the pressure (as Reynold's equation) and in the case of isothermal flow we have to determine the complete flowfield characterized by the air velocity $\mathbf{V}$ and the pressure P. The flow inside the 3D cells is governed by the Navier–Stokes system for compressible isothermal fluid

$$\frac{\partial\tilde{\rho}}{\partial t} + \nabla\cdot(\tilde{\rho}\mathbf{V}) = 0, \tag{1}$$

$$\tilde{\rho}\left[\frac{\partial\mathbf{V}}{\partial t} + (\mathbf{V}\cdot\nabla)\right]\mathbf{V} = -\nabla P + \mu\left[\nabla^2\mathbf{V} + \frac{1}{3}\nabla\nabla\cdot\mathbf{V}\right], \tag{2}$$

where μ is the shear viscosity and $\tilde{\rho}$ is the density. Also,

$$P = c_0^2\tilde{\rho}, \tag{3}$$

c_0 denoting the isothermal speed of sound in air. The origin is placed such that the z-axis is the symmetry line of the cell in the center of the circular hole (Fig. 4). The diaphragm lies in the plane $z=d$.

III. THE ANALYTIC SOLUTION

By linearizing Eq. (2) and assuming a time harmonic solution $\mathbf{V}(\mathbf{x},t)=\mathbf{v}(\mathbf{x})\exp(-i\omega t)$, $P(\mathbf{x},t)=p(\mathbf{x})\exp(-i\omega t)$, we obtain the Stokes' system,

$$\nabla\cdot\mathbf{v} = \frac{i\omega}{\tilde{\rho}_0 c_0^2}p, \tag{4}$$

$$-i\omega\tilde{\rho}_0\mathbf{v} = -\nabla p + \mu\left(\Delta\mathbf{v} + \tfrac{1}{3}\nabla\nabla\cdot\mathbf{v}\right), \tag{5}$$

where $\omega=2\pi f$, f being the frequency and $\tilde{\rho}_0$ being the unperturbed air density. The boundary conditions on the two bases have the form

$$u(\rho,d)=0 \quad w(\rho,d)=w^{(d)}(\rho), \tag{6}$$

$$u(\rho,0)=0, \quad w(\rho,0)=w^{(0)}(\rho), \tag{7}$$

where $(u(\rho,z),0,w(\rho,z))$ are the components of velocity $\mathbf{v}$ in the cylindrical coordinates (ρ,φ,z) and the function $w^{(0)}(\rho)$ is different from zero only in the opening (the hole surface of the top of the gap).

Particularly, in the case of a small and a medium radius hole, we write

$$w^{(0)}(\rho)=\begin{cases}\tilde{w}^{(0)}(\rho) & \text{if}\rho<r\\ 0 & \text{for } r<\rho<R,\end{cases} \tag{8}$$

$\tilde{w}^{(0)}(\rho)$ being an unknown function.

Remark 1. Conditions (6) and (7) are no-slip boundary conditions assuming a continuous flow. The fluid dynamics in a narrow domain between two parallel plates yields a decrease in pressure (rarefaction effect) which changes the boundary conditions on the solid surfaces giving a certain slip (tangential velocity) of the fluid particles.[22] The presence of perforations changes the pressure distribution in the gap area next to holes. It is clear that for perforated microstructures having the pitch of holes much larger than the air gap of the microstructure, the rarefaction is still in effect. But, if the pitch of holes is not much larger than the air gap, the presence of holes makes the slip of fluid particles on solid surfaces of the microstructure at least questionable. On the other hand, an elementary calculation shows that in the case of narrow circular pipes, of infinite extent, the direct hole resistance is not affected by the slip of the fluid particles on the wall. Also, as is shown in Ref. 21, the indirect hole resistance can be considered as a particular squeeze-film damping.

A. The equations for pressure and vorticity

We write Eq. (5) as

$$\mathbf{v}=\frac{1}{i\omega\tilde{\rho}_0}\left(1-\frac{\mu}{3}\frac{i\omega}{\tilde{\rho}_0c_0^2}\right)\nabla p-\frac{\mu}{i\omega\tilde{\rho}_0}\Delta\mathbf{v}. \tag{9}$$

By using the vectorial identity,

$$\nabla\times(\nabla\times\mathbf{v})=\nabla(\nabla\cdot\mathbf{v})-\nabla\mathbf{v}, \tag{10}$$

and taking into account the equation of continuity (4), there results

$$\mathbf{v}=\frac{\beta}{i\omega\tilde{\rho}_0}\nabla p+\frac{\mu}{i\omega\tilde{\rho}_0}\nabla\times\boldsymbol{\Omega}, \tag{11}$$

where

$$\beta=1-\frac{4i\omega\mu}{3\tilde{\rho}_0c_0^2}, \tag{12}$$

and

$$\boldsymbol{\Omega}=\nabla\times\mathbf{v} \tag{13}$$

is the vorticity. In the case

$$f\ll 3\tilde{\rho}_0c_0^2/(8\pi\mu)\approx 8.95\times10^8 \text{ Hz},$$

the second term in the right-hand side of formula (12) can be neglected resulting $\beta\approx1$.

In the axisymmetrical case, in the cylindrical coordinates, there is only one nonvanishing vorticity component

$$\nabla\times\mathbf{v}=\Omega\hat{\varphi}. \tag{14}$$

Thus, we obtain expressions for the velocities in terms of the pressure p and scalar vorticity Ω as potentials,

$$\mathbf{v}=\frac{\beta}{i\omega\tilde{\rho}_0}\nabla p+\frac{\mu}{i\omega\tilde{\rho}_0}\nabla\times(\Omega\hat{\varphi}). \tag{15}$$

This relationship can also be written as

$$u(\rho,z)=\frac{\beta}{i\omega\tilde{\rho}_0}\frac{\partial p}{\partial\rho}-\frac{\mu}{i\omega\tilde{\rho}_0}\frac{\partial\Omega}{\partial z}, \tag{16}$$

$$w(\rho,z)=\frac{\beta}{i\omega\tilde{\rho}_0}\frac{\partial p}{\partial z}+\frac{\mu}{i\omega\tilde{\rho}_0}\frac{1}{\rho}\frac{\partial(\rho\Omega)}{\partial\rho}, \tag{17}$$

where $u(\rho,z)$ and $w(\rho,z)$ are the nonvanishing components of the axisymmetrical velocity field in cylindrical coordinates. By applying in formula (15), the operator $\nabla\cdot$ and accounting of relationships (4), there results the partial differential equations satisfied by pressure

$$\frac{1}{\rho}\frac{\partial}{\partial\rho}\left(\rho\frac{\partial^2p}{\partial\rho}\right)+\frac{\partial^2p}{\partial z^2}+k^2p=0, \tag{18}$$

where the scalar wave number is

$$k=\frac{\omega}{c_0\sqrt{\beta}}. \tag{19}$$

Similarly, the application of operator $\nabla\times$ and consideration of formula (14) yields the vorticity equation,

$$\frac{1}{\rho}\frac{\partial}{\partial\rho}\left(\rho\frac{\partial\Omega}{\partial\rho}\right)-\frac{\Omega}{\rho^2}+\frac{\partial^2\Omega}{\partial z^2}+L^2\Omega=0, \tag{20}$$

L being the vector wave number,

$$L=\sqrt{i\omega\tilde{\rho}_0/\mu}. \tag{21}$$

B. Representation formulas for pressure, vorticity, and velocity fields

The separation of variables in Eqs. (18) and (20) associated with the condition of zero normal derivative of the pressure along the external cylindrical surface,

$$\frac{\partial p}{\partial n}(a,z)=0, \tag{22}$$

yields the representation formulas,

$$\frac{\beta}{i\omega\tilde{\rho}_0}p(\rho,z)=\phi_0(z)+\sum_{n=1}^{\infty}\phi_n(z)J_0(q_n\rho), \tag{23}$$

$$\phi_n(z) = A_0 \cos(kz) + \beta_0 \sin(kz),$$

$$\phi_n(z) = A_n \cosh(k_n z) + \beta_n \sinh(k_n z), \quad n \geq 1, \tag{24}$$

where the eigenvalues q_n are determined by

$$J_1(q_n R) = 0, \quad n = 0,1,2, \ldots, \tag{25}$$

and

$$k_n = \sqrt{q_n^2 - k^2}. \tag{26}$$

Also,

$$\frac{\mu}{i\omega\rho_0}\Omega(\rho,z) = \sum_{n=1}^{\infty} \Omega_n(z) J_1(q_n\rho), \tag{27}$$

where

$$\Omega_n(z) = C_n \cosh(r_n z) + D_n \sinh(r_n z), \tag{28}$$

and

$$r_n = \sqrt{q_n^2 - L^2}. \tag{29}$$

Formulas (16) and (17) yield the following representation formulas for the components of the velocity field:

$$u(\rho,z) = \sum_{n=1}^{\infty} u_n(z) J_1(q_n\rho), \tag{30}$$

where

$$u_n(z) = -q_n[A_n \cosh(k_n z) + B_n \sinh(k_n z)] - r_n[C_n \sinh(r_n z) + D_n \cosh(r_n z)], \tag{31}$$

and

$$w(\rho,z) = \sum_{n=0}^{\infty} w_n(z) J_0(q_n\rho). \tag{32}$$

The functions $w_n(z)$ have the expression

$$w_0(z) = k[-A_0 \sin(kz) + B_0 \cos(kz)], \tag{33}$$

$$w_n(z) = k_n[A_n \sinh(q_n z) + B_n \cosh(q_n z)] + q_n[C_n \cosh(r_n z) + D_n \sinh(r_n z)], \quad n = 1,2, \ldots. \tag{34}$$

The constants A_0, B_0, A_n, B_n, C_n, and D_n will be determined by using the boundary conditions (6) and (7).

1. Determination of constants

By using formulas (30) and (32) along the plane $z=d$, we can write

$$q_n[A_n \cosh(k_n d) + B_n \sinh(k_n d)] + r_n[C_n \sinh(r_n d) + D_n \cosh(r_n d)] = 0, \tag{35}$$

$$k_n[A_n \sinh(k_n d) + B_n \cosh(k_n d)] + q_n[C_n \cosh(r_n d) + D_n \sinh(r_n d)] = w_n^{(d)}. \tag{36}$$

Similarly, along the plane $z=0$, the u and w components of the velocity give

$$q_n A_n + r_n D_n = 0, \tag{37}$$

$$k_n B_n + q_n C_n = w_n^{(0)}, \tag{38}$$

$w_n^{(0)}$ and $w_n^{(d)}$ being the Fourier expansion coefficients corresponding to the functions $w^{(0)}(\rho)$ and $w^{(d)}(\rho)$:

$$w_n^{(0)} = \frac{2}{R^2}\int_0^r \tilde{w}^{(0)}(\rho)\rho \frac{J_0(q_n\rho)}{J_0^2(q_n R)} d\rho, \tag{39}$$

$$w_n^{(d)} = \frac{2}{R^2}\int_0^R w^{(d)}(\rho)\rho \frac{J_0(q_n\rho)}{J_0^2(q_n R)} d\rho. \tag{40}$$

Equations (35)–(38) determine the unknown pressure coefficients as

$$A_n = \mathbb{A}_n^{(0)} w_n^{(0)} + \mathbb{A}_n^{(d)} w_n^{(d)}, \tag{41}$$

$$B_n = \mathbb{B}_n^{(0)} w_n^{(0)} + \mathbb{B}_n^{(d)} w_n^{(d)}. \tag{42}$$

The coefficients $\mathbb{A}_n^{(0)}, \ldots, \mathbb{B}_n^{(d)}$ are defined by formulas

$$\mathbb{A}_0^{(0)} = \frac{\cot(kd)}{k}, \quad \mathbb{A}_0^{(d)} = \frac{\csc(kd)}{k}, \quad \mathbb{B}_0^{(0)} = \frac{1}{k}, \quad \mathbb{B}_0^{(d)} = 0, \tag{43}$$

$$\mathbb{A}_n^{(0)} = \frac{\sinh(k_n d)\cosh(r_n d) - \gamma_n \cosh(k_n d)\sinh(r_n d)}{k_n[2 - 2\cosh(k_n d)\cosh(r_n d) + [\gamma_n + \gamma_n^{-1}]\sinh(k_n d)\sinh(r_n d)]}, \tag{44}$$

$$\mathbb{A}_n^{(d)} = \frac{\gamma_n \sinh(r_n d) - \sinh(k_n d)}{k_n[2 - 2\cosh(k_n d)\cosh(r_n d) + [\gamma_n + \gamma_n^{-1}]\sinh(k_n d)\sinh(r_n d)]}, \tag{45}$$

$$\mathbb{B}_n^{(0)} = \frac{1 - \cosh(k_n d)\cosh(r_n d) + \gamma_n \sinh(k_n d)\sinh(r_n d)}{k_n[2 - 2\cosh(k_n d)\cosh(r_n d) + [\gamma_n + \gamma_n^{-1}]\sinh(k_n d)\sinh(r_n d)]}, \tag{46}$$

$$\mathbb{B}_n^{(d)} = \frac{\cosh(k_n d) - \cosh(r_n d)}{k_n[2 - 2\cosh(k_n d)\cosh(r_n d) + [\gamma_n + \gamma_n^{-1}]\sinh(k_n d)\sinh(r_n d)]}. \tag{47}$$

γ_n denotes

$$\gamma_n = \frac{k_n r_n}{q_n^2}.$$

C. One term approximations for the pressure and velocity in the opening

We assume that at the lower base of a hole the pressure has the form

$$p(\rho,0) = p_1^{(0)}, \quad \rho < r, \tag{48}$$

and that the velocity of the fluid,

$$w(\rho,0) = w^{(0)}, \quad \rho < r, \tag{49}$$

is also constant.

Particularly in the case of small holes the function $\tilde{w}^{(0)}(\rho)$ being a constant (49), a simple calculation based on formulas (A5) and (A6) yields

$$w_0^{(0)} = \frac{r^2}{R^2} w^{(0)}, \tag{50}$$

$$w_n^{(0)} = \frac{2r^2}{R^2} \frac{J_1(q_n r)}{q_n r} \frac{w^{(0)}}{J_0^2(q_n R)}, \quad n = 1,2,\ldots. \tag{51}$$

Remark 2. The one-term approximation for the pressure (48) and for velocity (49) assume small values of the radius r. For larger holes more terms have to be considered involving more unknown coefficients. However, the results obtained in Secs. IV and V show that the "one-term approximation" works well even in case of medium sized holes.

The equations of the problem are obtained now by using the representation formula (23) in condition (48):

$$\frac{\beta}{i\omega\tilde{\rho}_0} p_1^{(0)} = A_0 + \sum_{n=1}^{\infty} A_n J_0(q_n \rho), \quad \rho < r. \tag{52}$$

Equation (52) can be integrated with respect to ρ (between the limits 0 and ρ) yielding

$$A_0 \frac{\rho}{2} - \frac{\beta}{i\omega\tilde{\rho}_0} \frac{\rho}{2} p_1^{(0)} + \sum_{n=1}^{\infty} \frac{A_n}{q_n} J_1(q_n \rho) = 0, \quad \rho < r. \tag{53}$$

By substituting into Eq. (53), formulas (41) and (42), there results

$$\sum_{n=1}^{\infty} \left[\frac{\mathbb{A}_n^{(0)}}{q_n} w_n^{(0)} + \frac{\mathbb{A}_n^{(d)}}{q_n} w_n^{(d)} \right] J_1(q_n \rho) = -[\mathbb{A}_0^{(0)} w_0^{(0)} + \mathbb{A}_0^{(d)} w_0^{(d)}] \frac{\rho}{2} + \frac{\beta}{i\omega\tilde{\rho}_0} \frac{\rho}{2} p_1^{(0)}, \quad \rho < r. \tag{54}$$

Also, multiplying Eq. (54) by ρ^2 and integrating over $[0,r]$ give

$$\sum_{n=1}^{\infty} \left[\frac{\mathbb{A}_n^{(0)}}{q_n} w_n^{(0)} + \frac{\mathbb{A}_n^{(d)}}{q_n} w_n^{(d)} \right] \frac{J_2(q_n r)}{q_n r} = -[\mathbb{A}_0^{(0)} w_0^{(0)} + \mathbb{A}_0^{(d)} w_n^{(d)}] \frac{r}{8} + \frac{\beta}{i\omega\tilde{\rho}_0} \frac{r}{8} p_1^{(0)}. \tag{55}$$

Finally, the substitution of formulas (50) and (51) into relationships (55) gives the equation

$$w^{(0)} C_0 - \frac{\beta}{i\omega\tilde{\rho}_0} p_1^{(0)} = -\mathbb{A}_0^{(d)} w_0^{(d)} - \frac{8}{r} \sum_{n=1}^{\infty} \frac{\mathbb{A}_n^{(d)} J_2(q_n r)}{q_n^2 r} w_n^{(d)}, \tag{56}$$

where we have denoted

$$C_0 = \mathbb{A}_0^{(0)} \frac{r^2}{R^2} + \frac{16}{R^2 r} \sum_{n=1}^{\infty} \mathbb{A}_n^{(0)} \frac{J_1(q_n r) J_2(q_n r)}{J_0^2(q_n R) q_n^3}. \tag{57}$$

If the velocity of the diaphragm is constant, we have $w_n^{(d)} = w^{(d)} \delta_{n0}$ and the sum in right-hand side of Eq. (56) cancels out.

D. Determination of the velocity in opening

Using the impedance Z of the opening, we can write

$$p_1^{(0)} = -(Z + Z_C)\tilde{w}, \tag{58}$$

where Z_C is the acoustic impedance of the backchamber and $\tilde{w}$ is the algebraic volume velocity,

$$\tilde{\omega} = \pi r^2 w^{(0)}. \tag{59}$$

The acoustic impedance of the backchamber is[20]

$$Z_C = \frac{\gamma\tilde{\rho}_0 c^2}{i\omega V}, \tag{60}$$

where $\gamma = 1.403$ is the specific heat ratio of air and V denotes the volume of the backchamber. The impedance of the opening in the backplate is given in Ref. 23.

(1) Holes of very small diameter $r < 0.002/\sqrt{f}$,

$$Z = \frac{8\mu h}{\pi r^4} - i\omega \frac{4}{3} \frac{\tilde{\rho}_0 h}{3\pi r^2}. \tag{61}$$

(2) Intermediate-sized holes $0.01/\sqrt{f} < r < 10/f$,

$$Z \frac{\sqrt{8\omega\tilde{\rho}_0\mu}}{\pi r^2} \left(1 + \frac{h}{2r}\right) - i\omega\tilde{\rho}_0 \frac{h + 1.7r}{\pi r^2}. \tag{62}$$

Expression (62) includes also the end correction.

In the case of a hole whose radius lies between $0.002/\sqrt{f}$ and $0.01/\sqrt{f}$, interpolation must be used.

Equations (56), (58), and (59) permit determination of the pressure and velocity (assumed constants) in the opening. Particularly there results

$$w^{(0)} = W_0 w^{(d)}, \tag{63}$$

where,

$$W_0 = \left\{ k \sin(kd) \left[C_0 + \frac{Z + Z_C}{i\omega\tilde{\rho}_0} \beta \pi r^2 \right] \right\}^{-1}. \tag{64}$$

E. The analytic expressions for the damping coefficient and spring force

The pressure on the diaphragm can be written by means of formula (23) as

$$p(\rho,d) = \frac{i\omega\tilde{\rho}_0}{\beta} \left\{ A_0 \cos(kd) + B_0 \sin(kd) + \sum_{n=1}^{\infty} [A_n \cosh(k_n d) + B_n \sinh(k_n d)] J_0(q_n \rho) \right\}. \tag{65}$$

The total pressure (the pressure force) $P^{(d)}$ on the diaphragm results by integration with respect to θ and ρ:

$$P^{(d)} = -\frac{i\omega\tilde{\rho}_0}{\beta} \pi R^2 [A_0 \cos(kd) + B_0 \sin(kd)] = -\frac{i\omega\tilde{\rho}_0}{\beta} \frac{\pi R^2}{k \sin(kd)} \left[\frac{r^2}{R^2} w^{(0)} - \cos(kd) w^{(d)} \right]. \tag{66}$$

By introducing expression (63) of the velocity in the opening, we get

$$P^{(d)} = \frac{i\omega\tilde{\rho}_0}{\beta} \frac{\pi R^2 \cos(kd)}{k \sin(kd)} \left[1 - \frac{r^2}{R^2 \cos(kd)} W_0 \right] w^{(d)}.$$

Finally, the total damping coefficient of a cell B and the spring force coefficient S are

$$B + iS = \frac{i\omega\tilde{\rho}_0}{\beta} \frac{\pi R^2 \cos(kd)}{k \sin(kd)} \left[1 - \frac{r^2}{R^2 \cos(kd)} W_0 \right]. \tag{67}$$

This formula provides the total damping coefficient and the spring force coefficient on the developed model based on Stokes approximation of the viscous flow equations.

IV. AXIALLY SYMMETRIC NUMERICAL SIMULATION FOR VISCOUS DAMPING

The formula given by Škvor[8] (see also Refs. 24 and 25) assumes that the equivalent mechanical resistance of a cell (in lubrication approximation) is independent of frequency. The analysis of Zukerwar[20] shows that in the case of microphones in the audio frequency range, viscous damping is practically independent of frequency. The same conclusion was obtained in Ref. 26 in the case of an incompressible fluid as long as the frequency is smaller than 10^6 Hz. In this section, the viscous damping is modeled assuming weakly compressible fluid behavior for air. The squeezed flow is driven periodically in time and based on the above comments can be analyzed from the point of view of steady-state response.

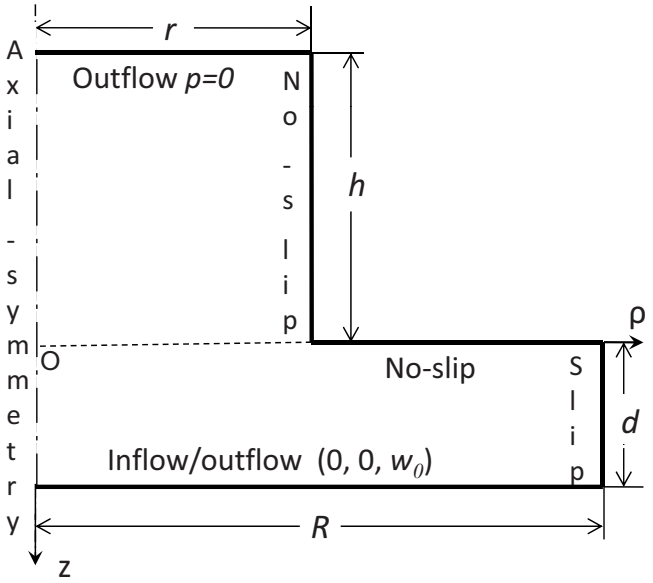

FIG. 5. The azimuthal section of the cell showing the dimensions and the boundary conditions.

The computational domain used here is the axisymmetrical region shown in Fig. 4. An azimuthal section of the cell showing the dimensions and the specified boundary conditions is given in Fig. 5. The bottom boundary corresponds to the diaphragm where the inflow/outflow condition $\mathbf{u} = (0,0,w_0)$ is specified. A constant pressure ($p=0$) outflow condition is specified along the top segment corresponding to the hole aperture. The no-slip condition is applied on solid surfaces (i.e., the wall of the hole and the lower surface of the backplate). Slip symmetry $\mathbf{V} \cdot \mathbf{n} = 0$ is specified along the outside cylindrical surface corresponding to the cell gap boundary. Finally, axisymmetry is specified along the central axis of the unit cell.

Solutions to the governing equations for the specified axisymmetric domain and boundary conditions were obtained using the weakly compressible Navier–Stokes application mode included in heat transfer module of COMSOL MULTIPHYSICS (Ref. 27) commercial software package. The software uses the finite element method for the spatial discretization of the governing equations (in cylindrical-polar coordinates). The domain is discretized using triangular elements. The COMSOL software employs an iterative procedure to solve the resulting discrete, nonlinear algebraic system of equations that result from the finite element approximation of the Navier–Stokes equations. A homogeneous, unstructured mesh was employed for most of the domain with areas of refinement in the gap region and around the re-entrant corner of the azimuthal domain. While the full Navier–Stokes equations were solved, for the conditions of the model here, the nonlinear terms are relatively small and accurate solutions are readily obtained. Grid convergence studies were performed starting with approximately 1000 elements and using up to as many as 20 000 elements for the most refined meshes.

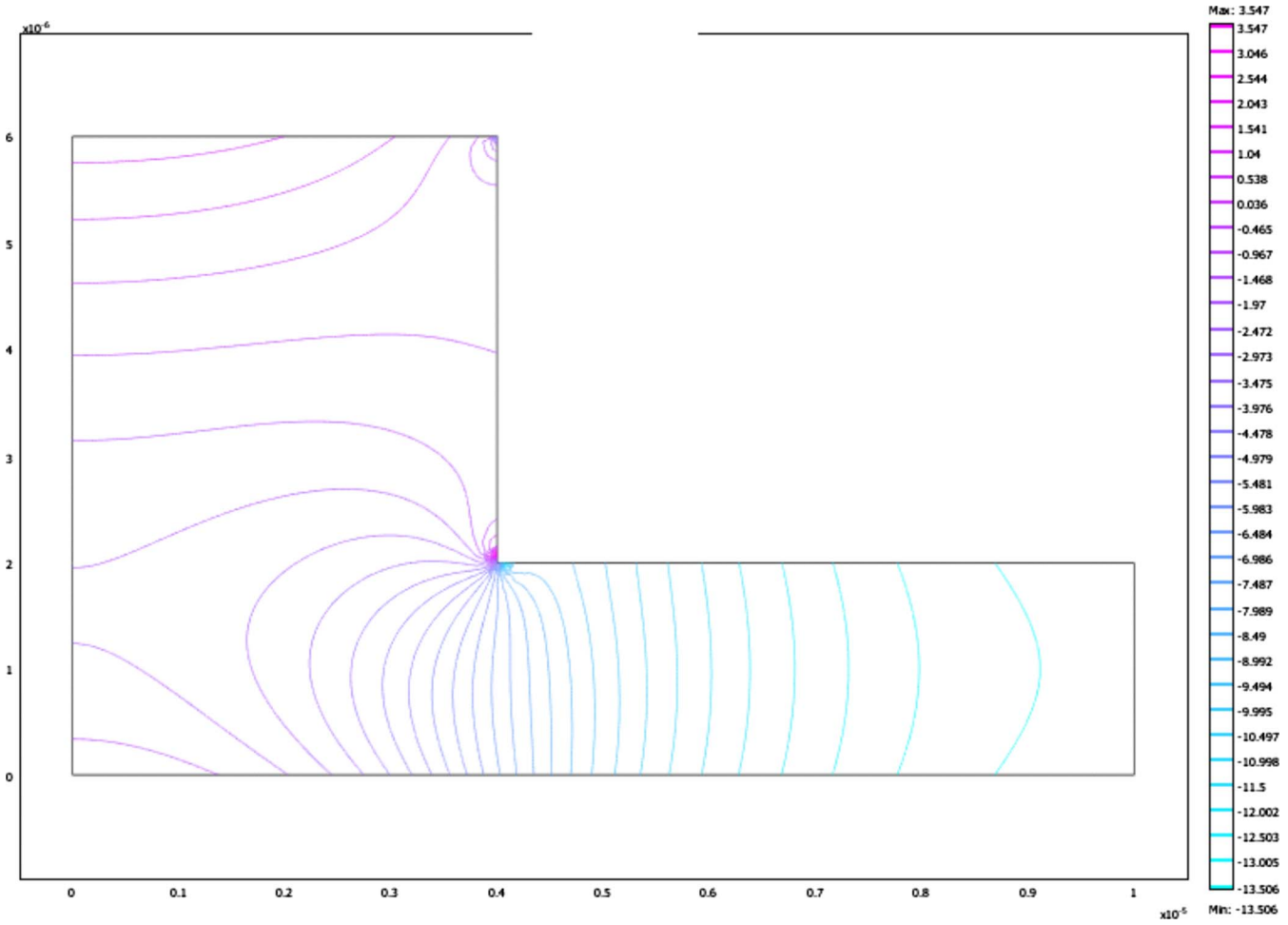

FIG. 6. (Color online) Contour plots of the pressure field in the azimuthal section resulted in numerical simulation.

Remark 3. In the numerical model presented here, standard continuum flow conditions have been assumed so that the no-slip condition applies along solid boundaries. In Ref. 16, both no-slip (models M1 and M2) and models with a slip velocity boundary condition (M3 and M4) were used along the walls in the air gap and the hole. If the scale of the flow is very small, then a slip model may be appropriate. However, for a gap on the order of 1 μm and an area ratio (area of the hole divided by the total area) around 50% half of the working area is open and rarefied gas behavior should not be important. In fact, some simple calculations show that in the case of a hole having a small radius and infinite length, the direct resistance of the hole is not influenced by the slip condition on the circular pipe. This geometry gives a redistribution of the pressure on the backplate very different from the rarefaction in a small gap between two parallel, nonperforated plane surfaces where a slip-flow may be a better model. This is evidenced by the fact that some of the results given in Table III in Ref. 16 are better when the standard continuum no-slip condition is applied along the solid surfaces. On the other hand, the indirect resistance of holes can be considered as a special squeezed film damping (see Ref. 21). See also the discussion in the book.[22]

Remark 4. In electrostatic-based transducers, application of voltages (polarization voltage for microphones and actuation voltage for actuators) is mandatory and this results in a static, nonlinear deflection of the diaphragm. In MEMS devices with very small air gap thickness, this can have a significant influence on the viscous damping. In the case of small deflections, the developed theory can be applied. For larger deflections, an axisymmetrical model can be obtained including the actual shape of the diaphragm and the FEM software will provide the viscous damping coefficient.

A. Sample results

Here we present a set of representative results by applying the axisymmetrical simulation and the analytical formula (67) to a unit cell with geometrical dimensions: $r=4$ μm, $R=8$ μm, $d=2$ μm, and $h=4$ μm. For the air in the unit cell, the following property values are used: density $\tilde{\rho}_0 = 1.155$ kg/m^3 and dynamic viscosity $\mu=18.5 \times 10^{-6}$ N s/m^2. As discussed above, a homogeneous, unstructured finite element mesh was used for the numerical computations with refinement around the re-entrant corner of the azimuthal domain. The total number of the finite elements is 9490 for the specific case presented here. Figure 6 shows contour plots of the pressure field (isobars) in the computational domain. An important element is the variation in the pressure in the axial direction (z). The result indicates

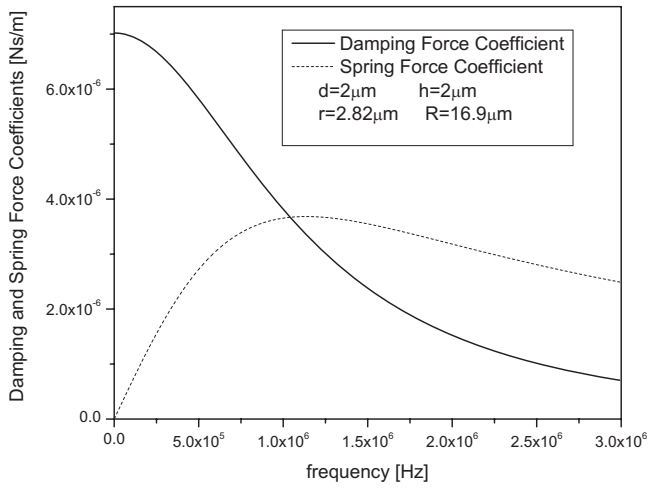

FIG. 7. Damping and spring force coefficients obtained by applying the analytical formula resulted by Stokes approximation.

a significant difference from the relationship $\partial p/\partial z=0$ assumed throughout the gap region in the lubrication type approaches.

From the numerical simulation for this case, the following values for the total damping coefficient of pressure force on the base $z=d$ of the cell (P) and the total damping coefficient of the total force (F_z) on the same base (including the viscous component) in the z-direction are obtained:

$$P = 1.058\,842 \times 10^{-7}\ \text{N s/m}, \tag{68}$$

$$B_{\text{num}} \equiv F_z = 1.058\,862 \times 10^{-7}\ \text{N s/m}. \tag{69}$$

These results show that the influence of the viscous force on the damping coefficient is very small compared with the pressure contribution. On the other hand, the calculation of the total damping coefficient as the sum of the hole resistance and the damping on the $z=0$ of the backplate gives an error of 0.23% as compared with the value given by the relationship (69).

Analytical formula (67) yields the following value of the damping coefficient:

$$B_{\text{STO}} = 1.1356 \times 10^{-7}\ \text{N s/m}, \tag{70}$$

resulting in a relative error of $e_{\text{STO}}=6.6\%$ with respect the value given by FEM simulation. The damping coefficient corresponding to the Reynolds approximation is

$$B_{\text{Rey}} = 6.15 \times 10^{-8}\ \text{N s/m}. \tag{71}$$

This value was obtained by adding the squeezed film damping given by Škvor's formula and the direct and indirect resistances of a hole defined in Ref. 21. The resulting value B_{Rey} has a relative error with respect to the FEM value of $e_{\text{Rey}}=42\%$.

The calculation of the total force on a cell by using the obtained analytical formula (67) was performed in the range of frequencies from 100 Hz to 3 MHz. The results are shown in Fig. 7, where the continuous line represents the damping force and the dotted line represents the spring force in the case where the effects of inertia and compressibility were included. The damping force dominates at low frequencies. The cutoff frequency is ≈ 1.5 MHz. For higher frequencies, the spring force is more important.

V. VALIDATION OF THE ANALYTICAL FORMULA

In this section, we compare the predictions from analytical solution and the FEM model to the published experimental data of Somà and De Pasquale.[28] In this cited paper, the details of the device configuration studied, the experimental setup, and the testing procedure are presented. The experimental configuration consists of a central suspended plate (where the structural stiffness is concentrated) covered with a pattern of square holes and connected to four lateral clamped supports of small cross-sectional area. This particular shape allows an out-of-plane deflection of lateral supports during the excitation and, consequently, a quasirigid oscillation of the central plate. The suspended plates are $h=15$ μm thick and have a gap of $d=1.6$ μm. Six different test configurations were studied: four specimens with different hole cross-sectional area size and two with the same hole dimensions but different plate widths. Table I gives the effective geometrical dimensions of the test structures obtained by profile measurements using an interferometric microscope. In the table, six cases are labeled A–F as in Refs. 16 and 28. The first four columns in Table I coincide with the corresponding columns in Table 1 of Ref. 16 including the plate length L, the plate width W, and the number of holes $M \times N$. Column five contains the perforation ratio q (same as the area ratio A) of the structure. In columns six and seven of Table I, we include the parameters b (the half-period of the structure) and $a=s_0/2$ (the half-length of a square hole side). Column nine contains the radius r of the circular cylinder which is equivalent to the square cross section of the hole of the test

TABLE I. The geometry of the measured and calculated structures.

Type	L (μm)	W (μm)	$M \times N$	q (%)	b (μm)	a (μm)	r (μm)	R (μm)
A	372.4	66.4	36×6	24	5.1	2.5	2.73	5.75
B	363.9	63.9	36×6	37	5.0	3.05	3.34	5.64
C	373.8	64.8	36×6	50	5.15	3.65	4	5.81
D	369.5	64.5	36×6	59	5.1	3.95	4.23	5.75
E	363.8	123.8	36×12	38	5.0	3.1	3.39	5.64
F	363.8	243.8	36×24	38	5.0	3.1	3.39	5.64

TABLE II. The measured, the analytical (Reynolds and Stokes) and computed damping coefficients.

Type	C_M measured (10^{-6} N s/m)	C_{Rey}-ΔRey (10^{-6} N s/m)-(%)	C_{STO}-ΔSTO (10^{-6} N s/m)-(%)	C_{num}-Δnum (10^{-6} N s/m)-(%)
A	47.38	33.82(−28.60%)	40.81(−13.88%)	40.46(−14.61%)
B	19.46	14.00(−28.10%)	18.30(−5.98%)	17.84(−8.32%)
C	9.863	7.57(−23.25%)	10.76(9.14%)	10.20(3.42%)
D	7.609	5.65(−25.81%)	8.095(6.39%)	7.650(0.54%)
E	38.22	26.35(−31.06%)	34.66(−9.30%)	33.74(−11.7%)
F	67.44	52.70(−21.86%)	69.32(2.89%)	67.48(0.06%)

specimen. Finally, the last column contains the radius R of the cylinder which substitutes the lower prism (gap region) of the domain.

In Ref. 28, the quality factor is determined from the experimentally obtained curve of displacement versus frequency, and the damping coefficient is then calculated from the quality factor, frequency, and the effective mass using the half-power bandwidth method. The values of the measured total damping coefficients, labeled as C_m, are given in column 2 of Table II for all six cases studied (note that this coincides with the second column in Table 3 of Ref. 28).

The columns 3–5 of Table II here contain the total damping coefficients C_{Rey}, C_{STO}, and C_{num} for the plate determined by multiplying the damping coefficient for a unit cell with the total number $M \times N$ of holes. In parenthesis in each case the relative error (ΔRey, ΔSTO, and Δnum) of the respective damping coefficient with respect to the measured value C_M was included. The coefficient c_{Rey} for a single cell was obtained by adding the squeezed film damping given by Škvor's formula and the direct and indirect resistances of a hole defined in Refs. 21 and 26. The coefficient c_{STO} is given by the real part of formula (67), while the coefficient c_{num} is obtained in numerical simulation as described in Sec. IV A.

It is clear that the results given by analytical formula are comparable with those obtained by finite element simulation and close to the measured values. Particularly, this validates directly the formula (67) for determining the damping and spring force for a cell. The precision of the analytical results are less in the case of perforated microstructures having a high area ratio. A better analytical approach in this case needs a more precise representation of the velocity in the opening. Also the total damping coefficient can be corrected by adding an edge correction to the boundary cells similar to the correction introduced in Ref. 21 for the case of the Reynolds' equation.

The results included in column 3 in Table II show that the Reynolds' lubrication model predictions fall below the results from the other two models. In some cases even the first digit of the total damping coefficient C_{Rey} is incorrect.

Table III presents the relative errors in the damping coefficient between the experimental values reported in Ref. 28, the four compact models presented in Ref. 16, and the relative error from the methods developed in this paper. The second column in Table III gives the relative error ΔM1 corresponding to the compact model M1 of Bao[10] for a rectangular damper that has a much larger length than width. The relative error values in column 3 (ΔM2) correspond to the model presented in Ref. 10 for an arbitrary rectangular surface. Columns 4 and 5 contain the relative errors (ΔM3 and ΔM4) of the compact models developed by Veijola:[5] model M3 corresponds to circular perforations of the backplate while model M4 was tailored specifically for square holes.[12] Column 6 includes the relative errors ΔSTO resulting from the use of the presented analytical formula and the last column includes the errors Δnum of the numerical simulation by the finite element method.

The results of numerical simulation given in this paper are in closer agreement with the measured values than those of the compact methods for all the microstructures considered. Also the values for the damping coefficient obtained by using the analytical formula for the damping coefficient of a cell compares well with the results reported in Ref. 16 for the compact models.

VI. CONCLUSIONS

A model for analyzing the viscous damping in a unit cell of a perforated microstructure has been developed. The model is based on the Stokes' equations for compressible, isothermal, viscous flow, and the approximation of the peri-

TABLE III. Relative errors of the compact models of analytical formula and of numerical simulation. The values ΔM1 – ΔM4 were given in Ref. 16.

Type	ΔM1 (%)	ΔM2 (%)	ΔM3 (%)	ΔM4 (%)	ΔSTO (%)	Δnum (%)
A	−23.53	−25.74	−33.51	−33.27	−13.88	−14.61
B	−16.36	−18.06	−21.02	−21.96	−5.98	−8.32
C	−5.21	−6.59	−4.11	−6.65	9.10	3.42
D	−14.66	−15.72	−12.46	−15.29	6.39	0.54
E	−17.27	−18.94	−19.03	−20.14	−9.30	−11.7
F	−4.77	−6.70	−5.19	−6.52	2.89	0.06

odic structure of common devices (squares or hexagonal prisms) by an equivalent axisymmetrical cylindrical domain. The analysis yields an analytical formula for the complex force (damping force and spring force) generated by the vibrating plate of the microstructure.

In addition, a FEM solution was used to determine the damping on the cell in the axisymmetrical domain.

The predictions for the damping coefficients from the analytical formula and numerical simulation were compared for some test microstructures and are found to be in good agreement. Also, these results are found to be in good agreement with some measured values found in the literature for some MEMS devices. This validates the model and demonstrates its broader range of applicability to real perforated microstructures. Also, the results obtained by these models compare well with the values given by some compact models in appropriate parameter ranges.

ACKNOWLEDGMENTS

This work has been supported by the National Institute on Deafness and Other Communication Disorders under Grant No. R01DC005762-05 for a NIH Bioengineering Research Partnership and Grant No. R01DC009429 to R.N.M.

APPENDIX: FINITE HANKEL TRANSFORMS AND MODIFIED FINITE HANKEL TRANSFORMS

In this appendix we prove the relationships (A5) and (A6) which are used in Sec. III A.

1. Some definitions and properties

We consider the finite Hankel transform of the function $u(\rho)$ with respect to ρ-variable defined by the relationship[29] (p. 83)

$$\tilde{u}(q_i) \equiv \tilde{\mathbb{J}}_1[u(\rho)] = \int_0^R u(\rho)\rho J_1(q_i\rho)d\rho, \tag{A1}$$

where q_i is a root of the transcendental equation

$$J_1(q_iR) = 0. \tag{A2}$$

At any point of $(0,R)$ at which the function $u(\rho)$ is continuous, the original function can be recovered by means of the inversion formula

$$u(\rho) = \frac{2}{R^2}\sum_i \tilde{u}(q_i)\frac{J_1(q_i\rho)}{[J_0(q_iR)]^2}, \tag{A3}$$

where the sum is taken over all the positive roots of Eq. (A2).

We define also the modified finite Hankel transform of the function $w(\rho)$ by formula

$$\hat{w}(q_i) \equiv \hat{\mathbb{J}}_0[w(\rho)] = \int_0^R w(\rho)\rho J_0(q_i\rho)d\rho. \tag{A4}$$

Inversion formula for the modified finite Hankel transform can be written as

$$w(\rho) = \frac{2}{R^2}\sum_{i=0}^{\infty} \hat{w}(q_i)\frac{J_0(q_i\rho)}{[J_0(q_iR)]^2}.$$

2. Calculation of some transforms

In the case of the function

$$f(\rho,r) = \begin{cases} \rho, & 0 \le \rho < r \\ 0, & r < \rho < R, \end{cases}$$

there results

$$\tilde{f}(q_ir) = \int_0^r \rho^2 J_1(q_i\rho)d\rho = r^3\int_0^1 t^2 J_1(q_irt)dt.$$

The last integral is given again by formula (6.567(1)) in Ref. 30. Therefore,

$$\tilde{f}(q_i,r) = r^3\frac{J_2(q_ir)}{q_ir}. \tag{A5}$$

In the case of the function,

$$h(\rho,r) = \begin{cases} 1, & 0 \le \rho < r \\ 0, & r < \rho < R, \end{cases}$$

there results

$$\hat{h}(q_i,r) = \int_0^r \rho J_0(q_i\rho)d\rho = r^3\int_0^1 tJ_0(q_irt)dt.$$

The last integral is given by formula (6.567(9)) in Ref. 30,

$$\hat{h}(q_i,r) = r^2\frac{J_1(q_ir)}{q_ir}. \tag{A6}$$

[1] J. J. Blech, "On isothermal squeeze films," J. Lubr. Technol. **105**, 615–620 (1983).
[2] T. B. Gabrielson, "Mechanical-thermal noise in micromachined acoustic and vibration sensors," IEEE Trans. Electron Devices **40**, 903–909 (1993).
[3] J. B. Starr, "Squeeze-film damping in solid-state accelerometers," in Proceedings of the IEEE Solid State Sensor and Actuator Workshop, Hilton Head Island, SC (1990), pp. 44–47.
[4] Y. J. Yang and S. D. Senturia, "Numerical simulation of compressible squeezed-film damping," in Proceedings of the IEEE Solid State Sensor and Actuator Workshop, Hilton Head Island, SC (1990), pp. 76–79.
[5] T. Veijola, "Analytic damping model for an MEM perforation cell," Microfluid. Nanofluid. **2**, 249–260 (2006).
[6] M. Bao and H. Yang, "Squeeze film air damping in MEMS," Sens. Actuators, A **136**, 3–27 (2007).
[7] C. W. Tan, Z. Wang, J. Miao, and X. Chen, "A study on the viscous damping effect for diaphragm-based acoustic MEMS applications," J. Micromech. Microeng. **17**, 2253–2263 (2007).
[8] Z. Škvor, "On acoustical resistance due to viscous losses in the air gap of electrostatic transducers," Acustica **19**, 295–297 (1967).
[9] T. Veijola and T. Mattila, "Compact squeezed-film damping model for perforated surface," in Proceedings of the Transducers '01, München, Germany (2001), pp. 1506–1509.
[10] M. Bao, H. Yang, Y. Sun, and P. J. French, "Modified Reynolds' equation and analytical analysis of squeeze-film air damping of perforated structures," J. Micromech. Microeng. **13**, 795–800 (2003).
[11] S. S. Mohite, V. R. Sonti, and R. Pratap, "A compact squeeze-film model including inertia, compressibility, and rarefaction effects for perforated 3-D MEMS Structures," J. Microelectromech. Syst. **17**, 709–723 (2008).
[12] T. Veijola, "Analytic damping model for a square perforation cell," in Proceedings of the Ninth International Conference on Modeling and Simulation of Microsystems, Boston (2006), Vol. **3**, pp 554–557.
[13] T. Veijola and P. Raback, "Methods for solving gas damping problems in

perforated microstuctures using a 2D finite-element solver," Sensors **7**, 1069–1090 (2007).
[14]S. S. Mohite, V. H. Kesari, V. R. Sonti, and R. Pratap, "Analytical solutions for the stiffness and damping coefficients of squeeze films in MEMS devices having perforated back plates," J. Microelectromech. Syst. **15**, 2083–2092 (2005).
[15]A. K. Pandey and R. Pratap, "A comparative study of analytical squeeze film damping models in rigid rectangular perforated MEMS structures with experimental results," Microfluid. Nanofluid. **4**, 205–218 (2008).
[16]T. Veijola, G. De Pasquale, and A. Somà, "Comparison between damping coefficients of measured perforated structures and compact models," in Proceedings of the DTIP, Nice (2008), pp. 236–241.
[17]D. H. Robey, "Theory of the effect of a thin air film on the vibrations of a stretched circular membrane," J. Acoust. Soc. Am. **26**, 740–45 (1954).
[18]I. G. Petritskaya, "Impedance of a thin layer of air in the harmonic vibrations of a membrane," Sov. Phys. Acoust. **12**, 193–198 (1966).
[19]I. G. Petritskaya, "Vibrations of a membrane loaded with a thin layer of air," Sov. Phys. Acoust. **14**, 105–106 (1968).
[20]A. J. Zuckerwar, "Theoretical response of condenser microphones," J. Acoust. Soc. Am. **64**, 1278–1285 (1978).
[21]D. Homentcovschi and R. N. Miles, "Viscous microstructural dampers with aligned holes: Design procedure including the edge correction," J. Acoust. Soc. Am. **122**, 1556–1567 (2007).
[22]G. Karniadakis, A. Beskok, and N. Aluru, *Microflows and Nanoflows* (Springer, Berlin, 2005).
[23]L. L. Beranek, *Acoustics* (McGraw-Hill, New York, 1954), p. 137.
[24]D. Homentcovschi and R. N. Miles, "Modelling of viscous damping of perforated planar micro-mechanical structures. Applications in acoustics," J. Acoust. Soc. Am. **116**, 2939–2947 (2004).
[25]D. Homentcovschi and R. N. Miles, "Viscous damping of perforated planar micromechanical structures," Sens. Actuators, A **119**, 544–552 (2005).
[26]D. Homentcovschi and R. N. Miles, "Analytical model for viscous damping and the spring force for perforated planar microstructures acting at both audible and ultrasonic frequencies," J. Acoust. Soc. Am. **124**, 175–181 (2008).
[27]COMSOL MULTIPHYSICS Version 3.5, http://www.comsol.com. (Last viewed 6/22/2009).
[28]A. Somà and G. De Pasquale, "Identification of test structures for reduced order modeling of the squeeze film damping in MEMS," Proceedings of the DTIP Symposium on Design, Test, Integration and Packaging of MEMS & MOEMS (2007), pp. 230–239.
[29]I. Sneddon, *Fourier Transforms* (McGraw-Hill, New York, 1951).
[30]I. S. Gradshteyn and I. M. Ryzhik, *Table of Integrals, Series, and Products* (Academic, New York, 1994).